MODELLING THE STRONG GROUND MOTIONS IN THE CITY OF PATRAS, GREECE, DURING JULY 1993 EARTHQUAKE

G-A. TSELENTIS*, G. KOUKIS**, E. SOKOS*, D. RUBAS*, J. JANSKY***, V. PLICKA***, M. PAKZAD***, AND J. ZAHRADNIK***

* Seismological Laboratory, University of Patras, Rio 261 10, Greece
** Laboratory of Engineering Geology, University of Patras, Rio 261 10, Greece
*** Department of Geophysics, Charles University, V Holesovickach 2, 180 00 Prague 8, Czech Republic

ABSTRACT

On July 14, 1993 a magnitude $M_s=5.4$ earthquake occurred close to Patras, Western Greece. Strong-ground motions recorded at two nearby stations B and C (with the maximum acceleration of 0.4g and 0.2g respectively) were analysed. The source and crustal propagation were modelled by the ray and discrete-wavenumber methods. For modelling the site effects, the finite-difference and matrix methods were used. The radially rupturing circular source of radius 3000 m explained not only the observed strong-motion duration, but also its composition of separate body wave arrivals, followed by surface waves. The peak velocity and acceleration pulses were identified as probably due to the rupture stopping. Although the calculated peak values are in an order-of-magnitude agreement with reality, the peaks at station B were twice as large as compared to those at station C. This could not be explained by the source and path effects, nor by the site effect. Strategy for resolving this discrepancy, and recommendations for practical implementation of the modelling in the prepared 'seismic scenario' of the Patras city were drawn.

KEYWORDS

Strong-ground motion, seismic scenario, seismic source, crustal propagation, site effects, discrete-wavenumber method, ray method, finite-difference method, matrix method.

INTRODUCTION AND DATA

On July 14, 1993 a magnitude $M_s=5.4$ (ISC) earthquake occurred a few kilometres from the city of Patras, Western Greece (Tselentis et al., 1994). Damages in the city, and availability of strong-motion records (maximum recorded acceleration 0.4g) have called for detailed studies, with the intention to identify relative roles of the source, crustal structure, and the local site structure during the strong ground motions. The studies represent a part of the prepared 'seismic scenario' (Tselentis et al., 1993), aimed to reduce losses due to future earthquakes. Considering the very high seismic potential of Western Greece (Papazachos, 1992), a great societal importance and an urgent need of such an undertaking are evident.

The focal parameters of the event (location and magnitudes) were determined from teleseismic and regional observations by ISC, NEIS, National Observatory of Athens, and PATNET=PATras seismic NETwork. The epicentre locations by these agencies agree well, and we use latitude=38.19°N, and longitude=21.76°E. As regards the focal depth, featuring a larger scatter, we prefer the local determination by PATNET, i.e. h=5 km. According to the Harvard calculation, the scalar seismic moment is $M_o=3.2 \cdot 10^{17}$ Nm. Assuming a stress

drop of 5MPa (reasonable for the Western-Greece events of this size, Melis *et al.*, 1995), we estimate the source radius to be R=3km. The Harvard double-couple focal mechanism solution of strike=238°, dip=73° and rake=-163° is assumed, because it is acceptable from the geological point of view. Together with the location, the focal mechanism suggests that the event was a manifestation of the recent activity of the Saravali fault (Tselentis *et al.*, 1994), shown in Fig. 1.

Fig. 1. The epicentre location of the studied event with respect to the causative fault, the coast, and the city of Patras (after Tselentis *et al.*, 1994). The borehole sites A, B, C, and D are also shown. The accelerographic stations were at B and C.

The crustal structure in Western Greece has been known from geophysical (Makris, 1977) and seismological studies (Panagiotopoulos and Papazachos, 1985; Pedotti, 1988; Melis *et al.*, 1989; Tselentis *et al* 1994). It is represented by a model consisting of 3 layers overlying a homogeneous halfspace, hereafter denoted as model M1 (Table 1). Details of the top 5km-thick layer have not been known so far, but sublayers of lower velocity, and/or velocity gradients in the upper part of the crust are geologically acceptable (Doutsos *et al.*, 1988). Therefore, two additional tentative models, progressively more complicated in the upper part, have been designed in this study; see MN1 and MN2 models in Table 1.

Table 1. Crustal models M1, MN1, and MN2, used in this study (Depth=depth of interface, V_p and V_s=the P and S-wave velocities, ρ=density, Qp and Qs=quality factors).

MODEL M1				
Depth (km)	V_p(km/s)	V_s(km/s)	ρ(kg/m³)	Qp=Qs
0	5.7	3.20	2840	300
5	6.0	3.37	2900	300
18	6.4	3.60	2980	300
39	7.9	4.44	3280	300
MODEL MN1				
0	2.67	1.50	2500	300
1	4.45	2.50	2500	300
2	5.7	3.20	2840	300
5	6.0	3.37	2900	300
18	6.4	3.60	2980	300
39	7.9	4.44	3280	300
MODEL MN2				
0	1.42	0.80	2500	300
0.5	2.67	1.50	2500	300
1	4.45	2.50	2500	300
2	5.7	3.20	2840	300
5	6.0	3.37	2900	300
18	6.4	3.60	2980	300
39	7.9	4.44	3280	300

The local structure at and around the accelerographic recording sites has been compiled from four boreholes, A,B,C,D of Fig. 1 and two cross-hole seismic measurements. The gross structure is represented by a 2D cross-section in Fig. 2, while more detailed 1D S-velocity models immediately below the strong-motion recording sites (B and C) are in Table 2. It is to stress that the site model has been rather uncertain so far. In particular, the cross-hole measurements indicated very large P/S velocity ratios, with a big scatter (from 3 to 10). The quality factors have not been measured at all.

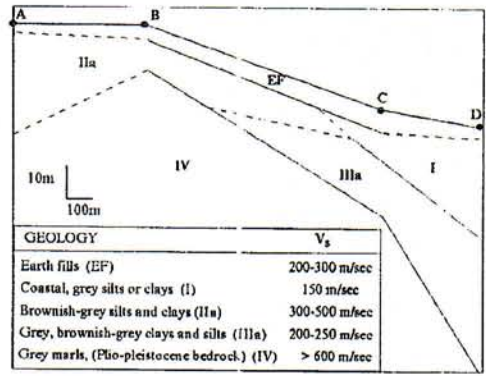| GEOLOGY	V_s
Earth fills (EF)	200-300 m/sec
Coastal, grey silts or clays (I)	150 m/sec
Brownish-grey silts and clays (IIa)	300-500 m/sec
Grey, brownish-grey clays and silts (IIIa)	200-250 m/sec
Grey marls, (Plio-pleistocene bedrock) (IV)	> 600 m/sec

Fig. 2. The geological cross-section along a profile connecting the boreholes A, B, C, and D.

The strong-motion data analysed in this paper consist basically of two three-component accelerograms at sites B and C (Lekidis et al., 1994). The accelerograms come from SMA-1 instruments, have been sampled at 0.005 s, and represent the corrected ground acceleration from 0.3 to 25Hz. We shall concentrate on the EW and NS components. As shown in Fig. 3, the accelerograms at sites B and C have similar shapes, but the peak value at site B (close to 0.4g) is twice as large as that at site C. The velocity time histories are depicted in Fig.4. The main difference between the velocity records at sites B and C is again their peak values. To further facilitate their modelling the velocigrams were low-pass filtered, using a window flat from 0 to 1 Hz, and cosine tapered between 1 and 2 Hz (Fig. 4a).

Between 3 and 6 seconds, i.e., within the hereafter called main wave group (i.e. the group dominating also the acceleration record), the B and C filtered velocity records are highly synchronous. This is contrasting with the following part of the record, a more low-frequency one, where the B and C records are out of phase, likely due to dispersion. This reason, and an additional one given below, suggest the interpretation of the main wave group as predominantly shear body waves, while the rest as predominantly surface and/or coda waves, hereafter denoted L. In this paper we concentrate just on the main (body) wave group. In the unfiltered records this group consists of three distinct arrivals, S1, S2, and S3.
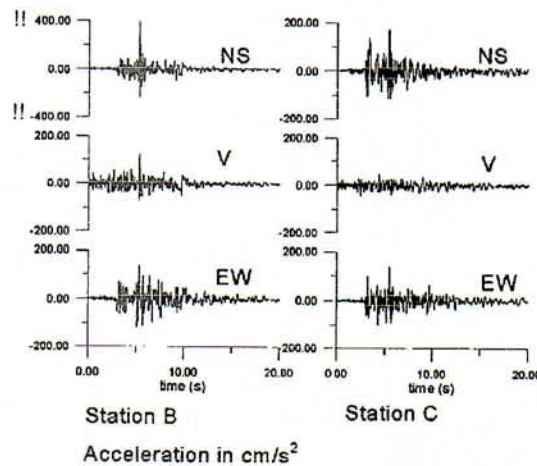

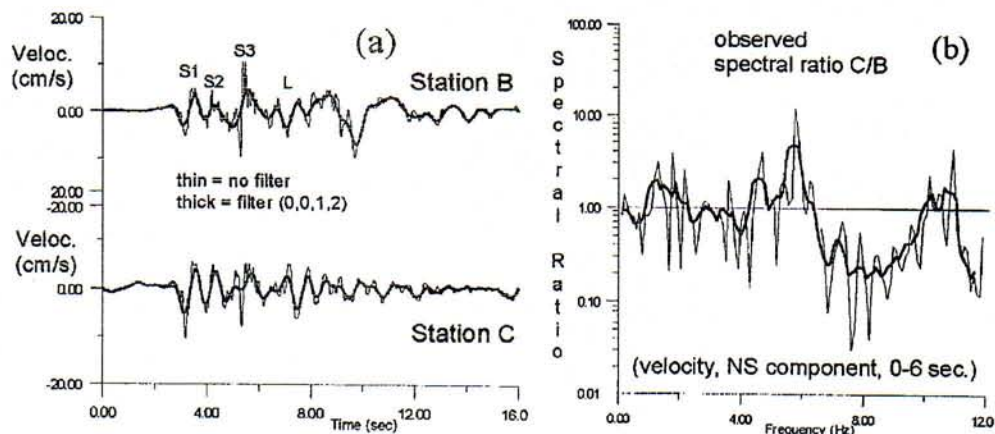Fig. 3. The acceleration time histories recorded at sites B and C.

Fig. 4 (a) The velocity-time histories (NS components) at sites B and C: nonfiltered (thin), and low-pass filtered up to 2 Hz (thick). Three distinct arrivals S1, S2, and S3 form the main wave group, which is then followed by L waves.

(b) The C/B spectral ratio (NS component) corresponding to the main wave group of the observed velocity time histories. Thin = before smoothing, thick = after smoothing.

Fig.4b depicts the amplitude spectra ratio of the ground velocities at station C with respect to that of station B. The ratio shows that amplification at station C with respect to B appears in the frequency band of 1-2 Hz and 4-6 Hz. On the contrary, beyond 6 Hz, the ground motion at station B is amplified. The latter behaviour is reflected in the time domain by the higher peak-motion values at station B.
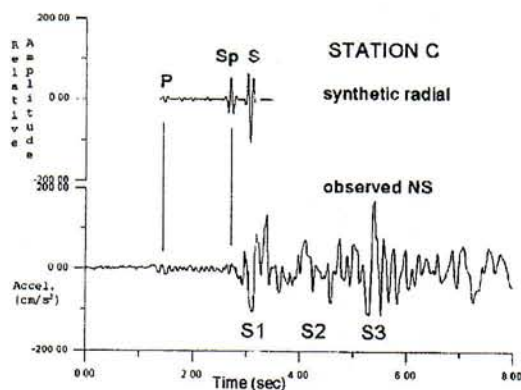

Fig. 5. Comparison between the ray synthetic for site C (the pseudoimpulse response) and the real record. The prominent arrivals of a known crustal path in model MN1 are identified.

Assuming a source radius of R=3 km, the expected corner frequency is at about 0.3 Hz. It is just at the lower edge of the frequency band of the recording instruments. Therefore, we are working in the band where all wavelengths are comparable or smaller than the characteristic source length. It means that the finite-source effects are inevitable. No filtration can move us into the band free of the finite-extent source effect. Also the epicentral distance is comparable to the fault length, thus enhancing the importance of the finite extent of the source.

MODELLING SOURCE AND CRUSTAL PROPAGATION

Based on the crustal models M1, MN1, and MN2 (Table 1), and assuming the Harvard focal mechanism, and variable source depths of 5, 7, and 10 km, the point-source synthetics were calculated by the ray method (Zednik et al., 1993). No site effects were considered at this stage. An artificial, short source duration was used to enhance the individual arrivals, preventing their overlap. The intention was to see the pseudoimpulse

response of the medium, not including effects of the fault size. Although a strong trade-off between the crustal structure and the source depth has been found, we concluded that the crustal models MN1 and MN2, and the source depth of 5 km, are acceptable for the available strong motion records (Fig. 5). Comparing the ray synthetics and the records we find that only few crustal phases significantly contribute to the observed ground motion. It is mainly the direct P wave, the Sp wave propagating most of its path as S, but (after refraction at the depth of 1 km) arriving at our stations as P, and the direct S wave. Therefore, the commencing part of the main wave group, S1, can be interpreted as a superposition of Sp and S. The rest, including the dominant phase S3, has no ray interpretation.

As a next step, a pseudoimpulse Earth's crust response, with the same point source and focal mechanism as above, and models M1, MN1, MN2 was calculated by the discrete-wavenumber method (Bouchon, 1981; Kennett and Kerry, 1979). An important result (not shown here) was that the stations B and C are close to the P-wave nodal plane. Therefore, any analyses of the S/P amplitude ratios would be highly unstable. The focal-mechanism effect upon the S-wave group has been found more stable, and well pronounced, suggesting a possible connection with the observed amplitude differences between the stations B and C. In contrast to the ray method, the individual elementary waves cannot be interpreted, because the method provides the complete wave field. On the other hand, all existing body and surface waves are automatically included. Thanks to the latter, a relatively long-period wave appeared in the synthetics, immediately following the S wave group, when using model MN2 (less in MN1, and not seen in M1). This fact contributed to our already mentioned interpretation of the L waves as surface waves.
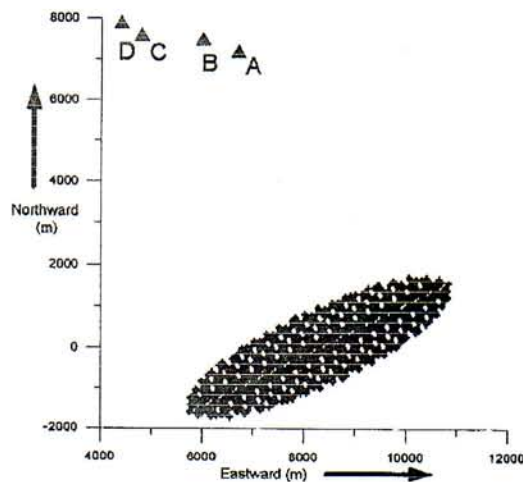

Fig. 6. The projection of the circular-source model onto the Earth surface, compared to the position of sites A, B, C, and D. The source radius is of 3000 m, and the rupture propagates radially form the centre (=hypocentre) at velocity of 2560 m/s. That is a dislocation model with a uniform (smooth-step) slip function, and rise time of 0.4 seconds all over the fault.

Considered hereafter is a circular source (Fig. 6), centred at the hypocentre, and fully contained within the fault plane. The rupture presumably starts at the hypocentre, and propagates radially at a constant velocity of 2560 m/s. We consider a dislocation model, the time function of the slip being the same everywhere, having form of a smooth step with rise time tentatively chosen as 0.4 seconds. The finite-extent modelling is realised by lagged summation of point sub-sources, distributed inside the circle within a square grid of 176m step. As the coherent source radiation needs sampling by minimum six sub-sources per shear wavelength at the source depth (Gariel et al., 1990), the step of 176m guarantees the coherent summation up to 3Hz, approximately. The synthetic velocigrams for such a source, embedded in the MN2 crustal model, are shown in Fig. 7. The peak values of the acceleration and velocity time histories synthetics on the L, T and Z components have been found of the same order of magnitude as peak values of the real records. The synthetics well display the presence of the L waves, and the duration of the main body wave group. Moreover, a peak appears now in the synthetics of Fig. 7 close to S3, allowing possible interpretation of that main body-wave arrival as due to the rupture stopping.

As the synthetics did not address frequencies higher than 3Hz (the limitation imposed in this paper by technical reasons only), they cannot provide explanation to the peak-amplitude differences of the acceleration records at stations B and C.
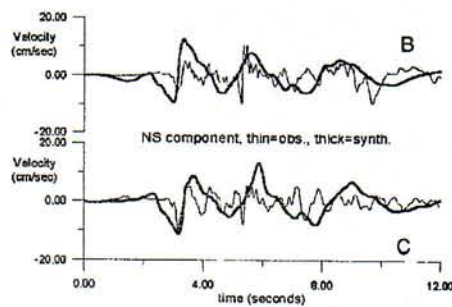
Fig. 7. The discrete-wavenumber synthetics for the radially rupturing circular-source model of Fig. 6. The synthetics (thick) are compared with real velocity records (thin).

MODELLING SITE EFFECTS

The 2D cross-section, containing the accelerographic stations B and C, has been subjected to the seismic-response analysis by the finite-difference method (Zahradnik and Priolo, 1995; Zahradnik *et al.*, 1991, 1994). The plane SV wave incident vertically from below was used as excitation of the site model. An artificial, short duration of the excitation was employed to get the pseudoimpulse response of the site, Fig. 8. Although no attenuation was considered at this moment, the site did not display any considerable 2D wave-propagation effect.

Table 2. Site models under accelerographic stations B and C (thickness of the layers, and their S-wave velocities).

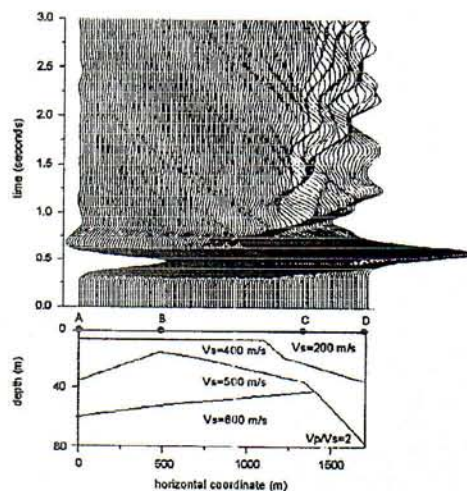| STATION B		STATION C	
thickness (m)	V_s (m/s)	thickness (m)	V_s (m/s)
4.5	250	6.8	250
9.0	400	9.8	150
38.3	300	17.3	225
halfspace	650	7.5	300
		halfspace	650

Fig. 8. The 2D finite-difference modelling (the pseudoimpulse response) at the cross-section A-D of Fig. 2. The horizontal component is displayed.

The response analysis in the 1D case, again assuming the vertical incidence of a plane S-wave, was performed by the matrix method (Muller, 1985; Zahradnik *et al.* 1991). Considering the 1D models below sites B and C (Table 2), the P-wave velocities are not needed for this study. The density of 2000 kg/m^3, and the quality factors Qp=20, Qs=10 were tentatively assumed. The transfer functions of these two sites were calculated, and the Fourier spectral ratios C/B constructed, Fig. 9. A good agreement between this theoretical ratio and the empirical ratio of Fig. 4b has been found for frequencies 1-2 Hz, where C/B > 1. Taking into account that in this frequency range the previously computed synthetics (not including the site effect) provided little differences between B and C, we conclude that below 2 Hz the B and C records can differ due to site effect.

On the other hand, for frequencies beyond 2 Hz, there is a considerable disagreement between the real and calculated spectral ratios. That is why the present 1D site models fail in explaining the observed larger peak motions at station B compared to C, in particular in the acceleration.
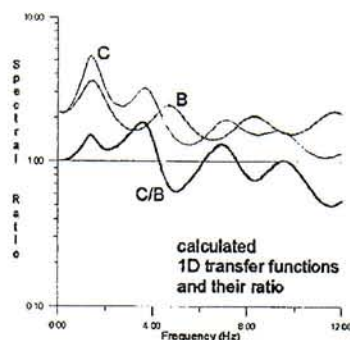

Fig. 9. The 1D matrix modelling of the spectral ratio C/B (thick) calculated as the ratio of the theoretical transfer functions C and B (thin).

CONCLUSION

The objective of this paper was to understand the strong-motion records obtained at two nearby sites in Patras, during the damaging earthquake of July 14, 1993. The available focal data were combined with the velocity models of the crust and of two recording sites. The seismic wave generation and the crustal propagation was then modelled by means of the ray and discrete-wavenumber methods. Finally, for modelling the site effects, the finite-difference and matrix methods were used. Comparing the synthetics with real records we have arrived to the following findings:

1. The main wave group of the record (i.e. that one prevailing in the acceleration- and velocity-time histories) is basically composed of Sp and S waves. The following part of the record is dominated by surface waves, L.

2. The duration of the main (body) wave group of the records can be explained by a circular source radially rupturing from the hypocenter. The assumed radius of R=3000 m, and the rupture velocity of 0.8 times shear velocity are acceptable. The peak velocity and acceleration pulses (S3) have been identified as probably due to the rupture stopping.

3. Peak values of the velocity and acceleration, obtained by modelling the source and crustal propagation effect (i.e., without the site effect) are in an order-of-magnitude agreement with the recorded peak values. However, in contrast to reality, they are not twice as large at B compared to C station.

4. A weak observed spectral amplification C/B for 1-2 Hz can be explained by the available 1D models of the near-surface structure below the stations. However, the 1D models do not explain the larger peak motions observed at station B compared to C, connected with the observed C/B < 1 for frequencies 2 to 4 Hz, and mainly beyond 6 Hz.

5. No pronounced 2D site effects have been found.

6. It remains not clear whether our failure in explaining the peak-motion differences between B and C comes from the source or site effect. The source effect cannot be ruled out, because our finite-source synthetics did not address frequencies larger than 3Hz. The site effect cannot be excluded too, because the site data were rather uncertain.

7. Two further steps are recommendable for improving the interpretation of the given records: (i) To calculate synthetics for the finite-extent source up to higher frequencies, (ii) To measure the C/B spectral ratios for more earthquakes, not necessarily the strong ones.

8. One step towards a practical application of the results is recommendable: to calculate the finite-source synthetics for many points in Patras up to 2 Hz, i.e. in the frequency range for which the present source and crustal model has been shown acceptable for stations B and C. Such a computational ground-motion mapping, would represent in fact a 'spatial extrapolation' of the Patras'93 strong-motion records into sites where the ground motion was also strong but not recorded. This may be useful for future antiseismic measures planned for the Patras city.

ACKNOWLEDGEMENTS

REFERENCES

Bouchon, M. (1981). A simple method to calculate Green's functions for elastic layered media. *Bull. Seism. Soc. Am.*, 71, 959-971.

Doutsos, T., Kontopoulos, N. and G. Poulimenos (1988). The Corinth-Patras rift as the initial stage of continental fragmentation behind an active island arc (Greece). *Basin Research*, 1, 177-190.

Gariel, J.-Ch., Archuleta, R.J. and M. Bouchon (1990). Rupture process of an earthquake with kilometric size fault inferred from the modelling of near-source records. *Bull. Seism. Soc. Am.*, 80, 870-888.

Kennett, B.L.N. and N. J. Kerry (1979). Seismic waves in a stratified half space. *Geophys. J. R. astr. Soc.*, 57, 557-583.

Lekidis, V., Margaris, V. and N. Theodulidis (1994). Strong motion characteristics and damage caused by two near field, moderate magnitude earthquakes in Greece (Pyrgos 26/3/93 and Patra 14/7/93). *ESC XXIV General Assembly*, September 1994, Athens, Greece.

Makris, J. (1977). Geophysical investigations of the Hellenides. Hamburger Geophys. Einzelschriften, 34 Wittenborn; Hamburg, Reihe A, 124pp.

Melis, N.S., Brooks, M. and R.G. Pearce (1989). A microearthquake network in the Gulf of Patras, western Greece, and its seismotectonic interpretation. *Geophys.J.R.astr.Soc.*, 98, 515-524.

Melis, N.S., Burton, P.W. and M. Brooks (1995). Coseismic crustal deformation from microseismicity in the Patras area. *Geophys. J. Int.*, 122, 815-836.

Muller, G. (1985). The reflectivity method: a tutorial. *J. Geophys.*, 58, 153-174.

Panagiotopoulos, D.G. and B.C. Papazachos (1985). Travel times of P_n waves in the Aegean and surrounding area. *Geophys. J. R. astr. Soc.*, 80, 165-176.

Papazachos, B.C. (1992). A time and magnitude predictable model for generation of shallow earthquakes in the Aegean area. *Pageoph*, 138, 287-308.

Pedotti, G. (1988). Etude sismotectonique du Peloponnese et reponse sismique d'une vallee sedimentaire en Grece du Nord. These, Universite Joseph Fourier, Grenoble.

Tselentis, G.-A., Karavolas, A., and C. Christopoulos (1993). The city of Patras - W. Greece: A natural seismological laboratory to perform seismic scenario practices. In: *Issues in Urban Earthquake Risk*, NATO ASI Series, Vol. 271, pp. 314-326.

Tselentis, G.-A., Melis, N., and E. Sokos (1994). The Patras (July 14; Ms=5.4) earthquake sequence. 7th Congress of the Geol. Soc. of Greece, Thessaloniki, May 25-27 (in press).

Zahradnik, J., J. Jech and V. Bartak (1991). Predicting ground-motion variations at the Turkey-Flat test site, California. *Pageoph*, 137, No. 1/2, 63-84.

Zahradnik, J., P. Moczo and F. Hron (1994). Blind prediction of the site effects at Ashigara Valley, Japan, and its comparison with reality. *Nat. Hazards*, 10, 149-170.

Zahradnik, J. and E. Priolo (1995). Heterogeneous formulations of elastodynamic equations and finite-difference schemes. *Geophys. J. Int.*, 120, 663-676.

Zednik, J., J. Jansky, and V. Cerveny (1993). Synthetic seismograms in radially inhomogeneous media for ISOP applications. *Computer & Geosciences*, 19, 183-187.